Development/Plasticity/Repair

Large-Scale Calcium Waves Traveling through Astrocytic Networks *In Vivo*

Nahoko Kuga,[1] Takuya Sasaki,[1] Yuji Takahara,[1] Norio Matsuki,[1] and Yuji Ikegaya[1,2]

[1]Laboratory of Chemical Pharmacology, Graduate School of Pharmaceutical Sciences, University of Tokyo, Tokyo 113-0033, Japan, and [2]Precursory Research for Embryonic Science and Technology, Japan Science and Technology Agency, Saitama 332-0012, Japan

Macroscopic changes in cerebral blood flow, such as those captured by functional imaging of the brain, require highly organized, large-scale dynamics of astrocytes, glial cells that interact with both neuronal and cerebrovascular networks. However, astrocyte activity has been studied mainly at the level of individual cells, and information regarding their collective behavior is lacking. In this work, we monitored calcium activity simultaneously from hundreds of mouse hippocampal astrocytes *in vivo* and found that almost all astrocytes participated en masse in regenerative waves that propagated from cell to cell (referred to here as "glissandi"). Glissandi emerged depending on the neuronal activity and accompanied a reduction in infraslow fluctuations of local field potentials and a decrease in the flow of red blood cells. This novel phenomenon was heretofore overlooked, probably because of the high vulnerability of astrocytes to light damage; glissandi occurred only when observed at much lower laser intensities than previously used.

Introduction

Astrocytes are biologically excitable. One form of the excitability is a change in the intracellular calcium concentration, which has been observed in cell cultures, brain slice preparations, and the *in vivo* neocortex and cerebellum. The intracellular calcium concentration in astrocytes increases both spontaneously and in response to neuronal activity and thereby modulates cerebral blood vessels (Iadecola and Nedergaard, 2007; Gordon et al., 2008; Giaume et al., 2010; Girouard et al., 2010), although the role of the calcium dynamics remains controversial (Fiacco et al., 2007; Agulhon et al., 2010; Hamilton and Attwell, 2010).

Most previous studies have addressed the action of astrocytes on the cerebrovascular system at the microscopic level of "single" astrocytes versus "single" vessels. Although sensory input-triggered or task-dependent activation of neurons is sparse in a brain subregion (Olshausen and Field, 2004; Ohiorhenuan et al., 2010; Wolfe et al., 2010), cerebral blood flow undergoes a massive change that occurs simultaneously among a number of blood vessels over the brain subregion; otherwise, blood flow changes would not be detectable as a net-averaged signal, such as the blood oxygen level-dependent (BOLD) signal in functional magnetic resonance imaging (fMRI). The BOLD signal supports the existence of currently unknown dynamics in multiple astrocytes that can widely regulate cerebral blood flow. However, to date, no studies have addressed large-scale behavior of astrocytes; note that, in previous studies, the activity of astrocytes *in vivo* has been recorded from only tens of cells in a small area. In the present study, we carefully monitored hundreds of astrocytes and discovered a novel ensemble behavior: virtually all the astrocytes in the field of view exhibited synchronous calcium activity, yielding a stereotypic traveling calcium wave ("glissando"). Notably, these large-scale events were associated with a reduction in infraslow local field activity and red blood cell (RBC) flow.

Received Oct. 10, 2010; revised Dec. 15, 2010; accepted Dec. 22, 2010.

This work was supported in part by a Grant-in-Aid for Science Research (KAKENHI 22115003, 22650080, and 22680025). We thank Y. Yamanishi for assistance with two-photon microscopy.

Correspondence should be addressed to Yuji Ikegaya at the above address. E-mail: ikegaya@mol.f.u-tokyo.ac.jp.

DOI:10.1523/JNEUROSCI.5319-10.2011

 0270-6474/11/312607-08$15.00/0

Materials and Methods

The experiments were performed with the approval of the animal experiment ethics committee at the University of Tokyo (approval numbers 19-37 and 19-39) and according to the University of Tokyo guidelines for the care and use of laboratory animals. Because there was no age-dependent difference in the properties of astrocytic glissandi, the data were pooled. The data represent the means ± SDs unless specified otherwise.

In vivo *calcium imaging of hippocampal astrocytes.* Male ICR mice (postnatal days 9–25) were anesthetized with urethane (1.5 g/kg, i.p.), and the exposed skull was glued to a metal plate, which was attached to a stereotaxic frame (see Fig. 1*A*). The mouse was placed on a heating pad (MATS-505SF; Thermo Plate; Tokai Hit), and its rectal temperature was kept at 34 ± 1°C (the temperature of the heat pad was set to be 37°C). Craniotomy (1–2.5 mm diameter), centered at 2.5 mm posterior and 2.2 mm lateral to the bregma, was performed, and the dura was surgically removed. As described by Mizrahi et al. (2004) and Sasaki et al. (2011), the cortical tissue above the dorsal hippocampus was removed by aspiration with extreme care to leave a small amount of the splenium of the corpus callosum above the alveus and to avoid damaging the hippocampal tissue (see Fig. 1*A*). The temperature inside the hippocampus was measured using a microprobe thermometer (BAT-12; Physitemp Instruments). The exposed surface was treated with 2 μl of a dye solution containing 0.125% fluo-4 acetoxymethyl ester (fluo-4 AM) (Invitrogen), 100 μM sulforhodamine 101 (SR101) (Invitrogen), 20% DMSO, and 8% Pluronic F-127 (Invitrogen). During an incubation period of 45–60 min, the aspirated surface was covered with Gel Form (Pfizer). Using this method, the fluo-4-loaded cells were almost exclusively SR101-positive astrocytes (see Fig. 1*B*) (Hirase et al., 2004). After the unloaded dye was washed away with artificial CSF (aCSF), the aspirated area was gently mounted with 2% agar dissolved in aCSF and covered with a coverslip.

The aCSF consisted of the following (in mM): 127 NaCl, 26 $NaHCO_3$, 1.6 KCl, 1.24 KH_2PO_4, 1.3 $MgSO_4$, 2.4 $CaCl_2$, and 10 glucose. The mouse on a stereotaxic frame was placed on the stage of an upright microscope (BX61WI; Olympus), and imaging was started ~30 min after the agar sealing. Astrocytic calcium activities were imaged at 1–10 Hz using a two-photon laser-scanning microscope (FV1000; Olympus). Fluorophores were excited by a mode-locked Ti:sapphire laser at 840 nm wavelength, 100 fs pulse width, and 80 MHz pulse frequency (Maitai HP; Spectra Physics). The laser beam was scanned by a galvano mirror. Fluorescent light was corrected by a water-immersion, high numerical-aperture (NA) objective lens (slow imaging: XLUMPLFL, 20×, 0.95 NA; fast imaging: ULTRA 25X MPE, 25×, 1.05 NA; Olympus). After blockade of the excitation light scattering with a 685 nm short-pass barrier filter, the fluorescence was separated through a FV10MP-MG/R filter (Olympus) and detected using a photomultiplier (r7862; Hamamatsu Photonics) controlled by FV10-ASW software (version 1.7; Olympus). The average size of the field of view was ~0.25 mm^2 (=500 × 500 μm). The laser intensity was measured above the specimen under the objective with a TB200 optical power meter (Yokogawa Electric). For the drug application, calcium activities were first monitored during a control period, and the agar covering the hippocampus was carefully removed. The hippocampal surface was perfused with the drug for 10 min and then remounted with 2% agar/aCSF containing the drug at the same concentration used for the perfusion. The drugs were dissolved in the agar solution immediately before mounting. For the local drug application, the drugs were dissolved in aCSF containing 0.1% Alexa Fluor 568 and loaded into borosilicate glass pipettes (5–7 MΩ). They were ejected using positive pressures of 50–100 hPa. Carbenoxolone, suramin, tetrodotoxin, (*S*)-α-methyl-4-carboxyphenylglycine (MCPG), and 8-cyclopentyl-1,3-dipropylxanthine (DPCPX) were purchased from Sigma-Aldrich. Electric stimulation (100 pulses at 100 Hz, 100 μs rectangular pulses at 100 μA) was administered through a monopolar glass electrode (7–9 MΩ), except for DPCPX. DPCPX was intravenously injected through a caudal vein. After each experiment, the brain was removed and fixed immediately. Coronal sections (30 μm thickness) were stained with 0.1% cresyl fast violet (Wako Pure Chemical Industries) to assess the imaged area (see Fig. 1*A*). Only data obtained from the hippocampal CA1 region were used for analysis.

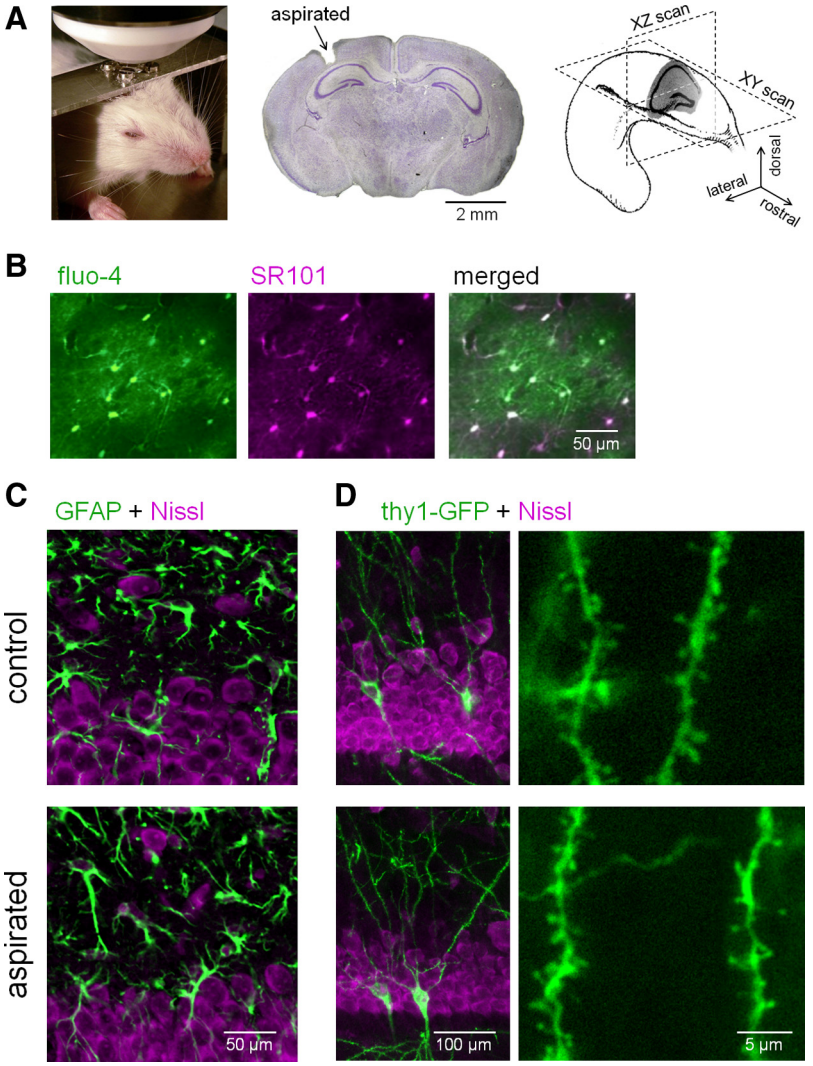

Figure 1. *In vivo* two-photon imaging of hippocampal astrocyte population. ***A***, Two-photon images of astrocytes were obtained in an *XY* or *XZ* plane of the hippocampus in a head-restrained, urethane-anesthetized mouse. The middle photograph shows a Nissl-stained coronal section in which a small portion of the cerebral cortex has been aspirated to optically access the hippocampus. ***B***, Two-photon images of cells loaded with SR101 and fluo-4. Fluo-4-loaded cells were positive for SR101, an astrocyte-specific marker. ***C***, Comparison of GFAP-positive cells in the hippocampal CA1 stratum oriens between aspirated (bottom) and the contralateral (control; top) side. Fluorescent Nissl (magenta) was used for counterstaining. Neither an abnormal morphology nor an upregulation of GFAP occurred after aspiration. ***D***, Comparison of Thy1-GFP-positive cells in the hippocampal CA1 stratum oriens between the aspirated side and the contralateral control side. Magnified images of the Thy1-GFP-positive basal dendrites are shown in the right panels. Neither dendritic swelling nor spine loss was induced by aspiration.

Analysis of calcium dynamics. Based on SR101 fluorescence, astrocyte cell bodies were carefully identified macroscopically to determine the regions of interest (ROIs). To minimize signal contamination from astrocytic processes, the ROI size was set to 10 μm in diameter, which corresponds to the soma size of an astrocyte. In each ROI, the fluorescence intensity was spatially averaged for each movie frame. The fluorescence change was defined as $\Delta F/F = (F_t - F_0)/F_0$, where F_t is the fluorescence intensity at time t, and F_0 is the baseline average for 50 s around the focused time t. Calcium increase events were detected with thresholds of 4 × SDs of the baseline noise and a 5 s duration. The timings of the onset of calcium events are presented in rastergrams.

Cell morphology. After the imaging experiments, the mice were perfused transcardially with chilled PBS followed by 4% paraformaldehyde in 0.1 M phosphate buffer, pH 7.4. The brains were removed, fixed in 4% paraformaldehyde overnight at 4°C, and coronally sectioned at a thickness of 20 μm using a cryostat (Microm HM520; Thermo Fisher Scientific). For immunostaining, the sections were permeabilized with 0.1% Triton X-100 and 5% goat serum diluted in 0.1 M phosphate buffer at room temperature for 10 min. Next, they were incubated with primary rabbit polyclonal antibody against glial fibrillary acidic protein (GFAP) (1:400; Z0334; Dako) or ionized calcium-binding adapter molecule 1 (Iba1) (1:400; 019-19741; Wako Pure Chemical Industries) overnight at room temperature and labeled with Alexa Fluor 488-conjugated anti-rabbit IgG secondary antibody (1:400; Invitrogen) and Nissl Red (1:200; Invitrogen) for 3 h at room temperature. Dendrites were visualized in brain sections prepared from mice expressing membrane-targeted green florescent protein (GFP) (line 21; Thy1-GFP transgenic mice), a gift from Dr. V. de Paola and Dr. P. Caroni (the University of Basel, Basel, Switzerland) (De Paola et al., 2003). Images were acquired at a *Z*-depth interval of 0.5 μm using a FV1000 confocal laser-scanning system with a BX61WI upright microscope (Olympus) and a water-immersion objective lens (XLUMPLFL; 40×, 0.95 NA, 2× optical zoom; Olympus).

Electrophysiological recordings. Local field potentials (LFPs) were recorded from the CA1 stratum pyramidale. Borosilicate glass capillaries with inner filaments (CG-1.5; Ken Enterprise) were pulled (1–2 MΩ) with a P-97 puller (Sutter Instrument) and filled with aCSF. Recordings were amplified using MultiClamp 700B (Molecular Devices) and analyzed with Clampex 10.2 (Molecular Devices). Signals were digitized at 10 kHz.

Blood flow imaging. In the fluo-4-loaded mice, blood serum was labeled with intravenous injection of 30–250 μl of 1% fluorescein isothiocyanate-labeled dextran (FITC-dextran) (70 kDa) in saline. The dye was injected repeatedly as required to cancel the photobleaching and dye metabolism. The capillaries of interest were XT-scanned along their longitudinal axes using the two-photon microcopy system (Kuga et al., 2009). The pixel rate was 10 or 20 μs, and the time resolutions were 0.7–3.4 ms per X-scan line. The velocity of each RBC was measured as an angle of its oblique "shadow" band (see Fig. 7*D*). This method is usable particularly in measuring the flow of capillaries, because RBCs in larger vessels sometimes pass obliquely through an out-of-focus depth of field, leading to an inaccurate estimation of the RBC velocity. Thus, capillaries with 5–8 μm diameters were selected for imaging.

Results

In vivo imaging of hippocampal astrocytes

Two-photon images were obtained to evaluate the calcium activity in astrocytes in the hippocampi of anesthetized mice (Fig. 1*A*). The neocortex covering the dorsal hippocampal CA1 region was aspirated with extreme care (Mizrahi et al., 2004), and the exposed tissue was treated with fluo-4 AM and SR101, a specific marker of astrocytes (Nimmerjahn et al., 2004). Using this dye permeation method (Hirase et al., 2004), fluo-4 was incorporated almost exclusively into astrocytes (Fig. 1*B*).

The aspiration per se was unlikely to cause tissue damage in the hippocampus, based on the five following observations: (1) We compared the immunoreactivity of GFAP in CA1 stratum oriens and stratum pyramidale of the imaged hippocampus with that in the contralateral, nonaspirated side. We did not detect an abnormal morphology of the astrocytes or an upregulation of GFAP expression, which is indicative of reactive astrocytes (Fig. 1*C*). (2) Neither aberrant swelling nor spine loss was observed in the basal dendrites of CA1 pyramidal cells (Fig. 1*D*). Note that both phenomena are highly responsive signs of tissue damage (Ikegaya et al., 2001). (3) No apparent activation of microglia, assessed by anti-Iba1 immunostaining, was observed (supplemental Fig. S1, available at www.jneurosci.org as supplemental material). (4) Consistent with Dombeck et al. (2010), theta oscillations and ripple waves, electric field oscillations typical of the *in vivo* hippocampus, were normally recorded from the exposed hippocampus (supplemental Fig. S2, available at www.jneurosci.org as supplemental material). (5) The intrahippocampal temperature was not different between the aspirated brain (31.3 ± 0.4°C; $n = 3$ mice) and the intact brain (30.8 ± 0.8°C; $n = 3$ mice). Incidentally, these temperatures were lower than the rectal temperature (34 ± 1°C). This may be because we did not directly control the brain temperature in anesthetized animals.

We recorded the spontaneous calcium activity of astrocytes in the CA1 stratum oriens at one frame per second in horizontal *XY*-scan mode (Fig. 2*A–C*). The tissues were illuminated with two-photon lasers at the weakest intensities possible while maintaining signal-to-noise ratios >7 dB (Fig. 2*B*, <10 mW). Single movies included 116 ± 43 astrocytes, ranging from 29 to 221 astrocytes ($n = 90$ mice). In all the movies, we observed that the astrocytes spontaneously generated sporadic calcium activities. In 30 of 90 mice (33%), however, we detected intermittently synchronized calcium activities (Fig. 2*C*). The probability of observing the synchronized events did not differ depending on the ages of animals [postnatal day 9 (P9) to P25] (supplemental Fig. S3*A*, available at www.jneurosci.org as supple-

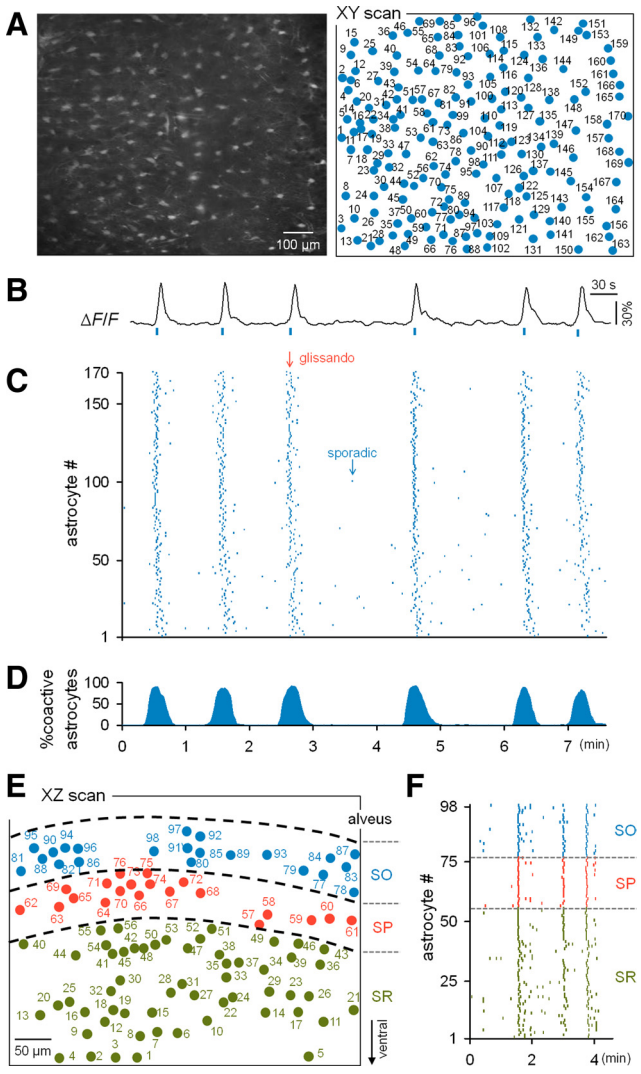

Figure 2. Calcium activities of astrocytes that were synchronized throughout the dorsal hippocampus. ***A***, Two-photon image of an *XY* section of the stratum oriens in a fluo-4-loaded hippocampus (left) and the identified location of the somata of individual astrocytes. ***B***, Typical trace of the calcium fluorescence intensity of a single astrocyte. ***C***, Rastergram of the astrocytic activities recorded in ***A***. Each dot indicates the timing of a single calcium event. Synchronous activities (glissandi) were evident in the background of sparse activities (sporadic). ***D***, Percentage of active astrocytes at a given time (10 s bin). ***E***, Map of astrocytes in an *XZ* section across the stratum oriens (SO), stratum pyramidale (SP), and stratum radiatum (SR) in the hippocampus. ***F***, Rastergram of the astrocytes shown in ***E***.

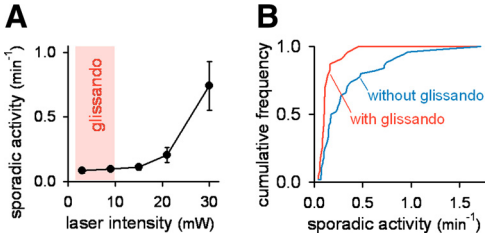

Figure 3. Glissandi are light-vulnerable. ***A***, The relationship between the mean frequency of sporadic activities and the light intensity of the laser used for imaging. The activities increased with the laser intensity, and glissandi occurred only at the weakest laser intensities (shaded zone). Error bars indicate SD. ***B***, Preparations that exhibited glissandi had lower frequencies of sporadic activity compared with those that did not demonstrate glissandi. Data are a compilation of 72 movies (35 mice; laser intensity, 8–30 mV).

mental material). In animals that exhibited the synchronized events, the events were stably observed at a frequency of ~0.3 events/min, and their frequencies did not change at least during our observation period of up to 150 min (supplemental Fig. S3*B*, available at www.jneurosci.org as supplemental material).

The synchronized activities were large events that recruited virtually all the astrocytes in the microscopic field of view (Fig. 2*D*; supplemental Movie 1, available at www.jneurosci.org as supplemental material). These large-scale events were also observed in dorsoventral *XZ*-scanned movies that included the CA1 stratum oriens, the stratum pyramidale, and the stratum radiatum (Fig. 2*E*,*F*) ($n = 10$ events from three mice). The synchronous events were therefore likely to involve the entire CA1 region of the dorsal hippocampus. The synchronization duration was, on average, 36 ± 24 s ($n = 132$ events from 10 mice), but it varied among events, ranging from 16 to 113 s; short events usually consisted of single synchronous activities, whereas longer ones that persisted for >1 min involved a few synchronous activities (for example, see Fig. 5*A*).

Why was this obvious phenomenon previously unknown? This oversight may be attributed to difficulties associated with optical imaging; that is, astrocytes are light-excitable (Parpura et al., 1994; Wang et al., 2006). The frequency of background ("sporadic") activity increased with the intensity of the two-photon laser (Fig. 3*A*). Synchronized events were observed only when sporadic activities were present at low frequencies (Fig. 3*B*). More practically, the synchronization occurred only when movies were obtained at laser intensities <10 mW (Fig. 3*A*). It should be noted that even researchers who recognized the light sensitivity of astrocytes have routinely used laser intensities >20 mW (for example, see Wang et al., 2006; Takata and Hirase, 2008; Nimmerjahn et al., 2009). It should also be noted that, in Figure 2*D*, we used laser powers of >20 mW to take *XZ*-scanned movies. In this case, the synchronization disappeared soon (within a few minutes) after observation, and we were able to record only 10 events from three mice. Importantly, preparations that displayed a low level of sporadic activities did not always exhibit synchronization. This result may reflect intrinsic brain state fluctuations or suggest that our laser intensities were still too high and sometimes disturbed the ensemble dynamics of astrocytes.

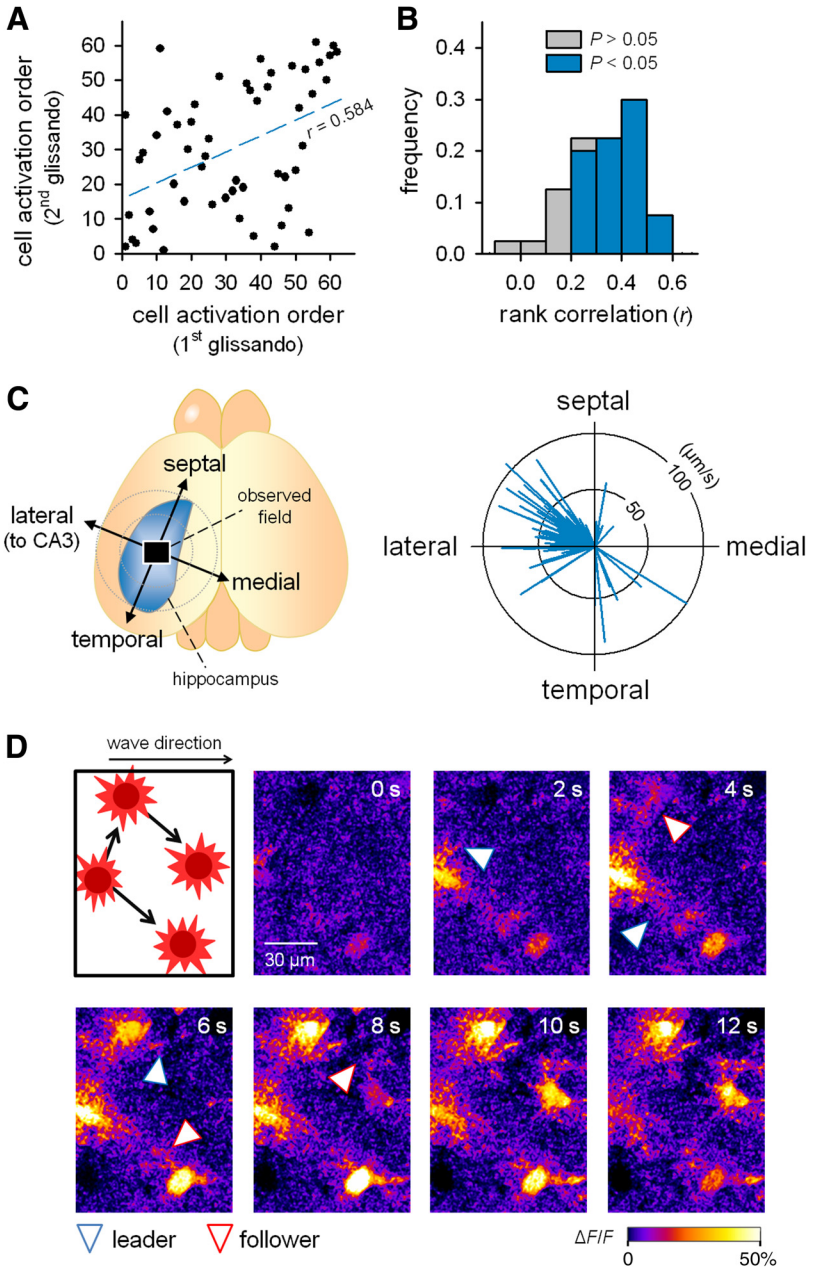

Figure 4. Glissandi propagate from foot to foot in the CA1 to CA3 direction. ***A***, Representative sequential plot showing the activation order of astrocytes in two successive glissandi (first glissando and second glissando). Each dot indicates a single astrocyte. The movie was obtained at 10 Hz to determine the precise order of cell activation. Spearman's rank correlation coefficient (*r*) was 0.584. ***B***, Summary of the correlation coefficients for all pairwise data. Among 40 pairs in five glissandi, 32 (80%) exhibited a significance level of 5% for the rank correlation (colored). ***C***, The direction and speed of glissandi were calculated using a linear regression and vector-plotted in the right circle graph. Each vector represents a single glissando, and its orientation and length indicate the direction and speed of propagation ($n = 38$ glissandi, 8 mice). ***D***, Two-photon imaging with a higher magnification and a higher numerical aperture objective (25×, 1.05 NA) revealed that calcium activity propagated from a leader foot of one cell to the neighboring follower foot of another cell during the propagation of a glissando. The blue and red arrowheads indicate leader feet (donors) and follower feet (recipients), respectively. Similar microscopic patterns of propagation were observed in all three animals tested.

Astrocytic glissandi

Higher-speed (10 Hz) imaging revealed that the synchronous events were wave-like propagations that spread from cell to cell. The mean speed of the propagation was 61 ± 22 μm/s ($n = 38$ events from eight mice). We termed these calcium waves "glissandi," because they did not bear a resemblance to any previously described waves (as discussed below). The sequential order of activity in individual astrocytes during glissandi varied from event to event (Fig. 4*A*), but as a whole, the orders were positively correlated among events (Fig. 4*B*). In accord with this finding, glissandi propagated almost consistently in the medial-to-lateral direction toward the CA3 region (Fig. 4*C*). Using imaging at

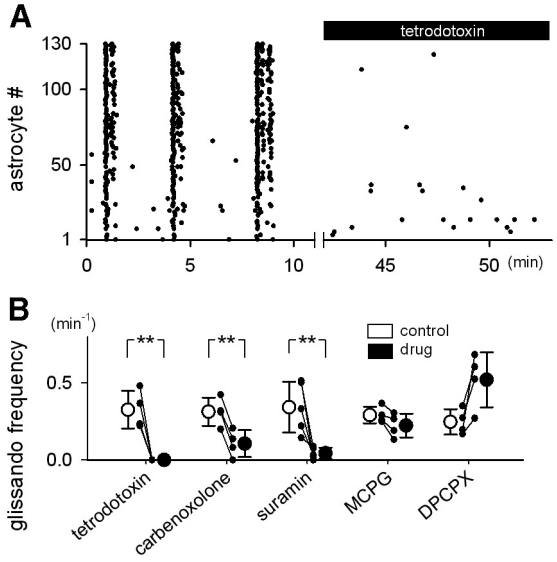

Figure 5. Glissandi depend on neuronal activity, ATP receptors, and gap junctions. ***A***, After monitoring glissandi under control conditions, the alveus surface of the hippocampus was treated with 2 μM tetrodotoxin, and the astrocytes were reobserved. Tetrodotoxin blocked the generation of glissandi. ***B***, Summary of the pharmacological characterization. Glissandi were inhibited by tetrodotoxin (2 μM; $n = 4$ mice), carbenoxolone (250 μM; $n = 4$ mice), and suramin (1 mM; $n = 5$ mice), but not by MCPG (1 mM; $n = 4$ mice) or DPCPX (1 mg/kg, i.p.; $n = 4$ mice). $^{**}p < 0.01$ versus control, paired t test. Error bars indicate SD.

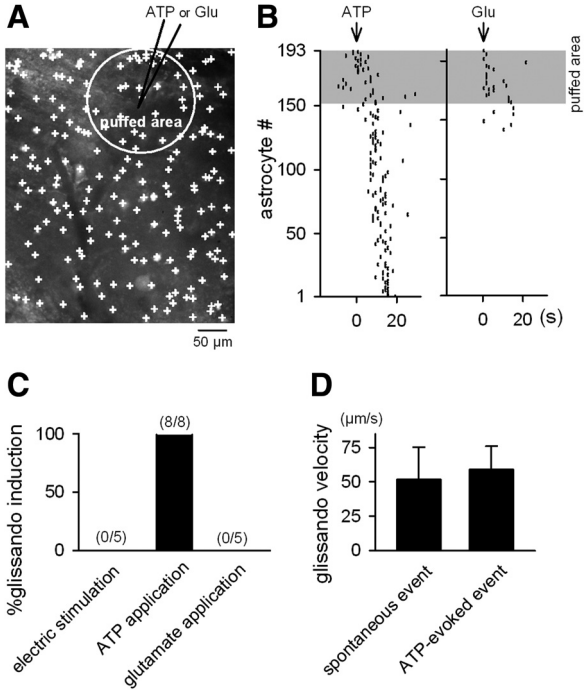

Figure 6. Local application of ATP evokes glissandi. ***A***, An *XY*-scan image of astrocytes in the CA1 stratum oriens, in which a glass pipette (7–9 MΩ) loaded with 1 mM ATP or 1 mM glutamate (Glu) was inserted into the CA1 stratum pyramidale. The agonists were pressure-ejected, and the puffed area was identified by spread of fluorescence of the coapplied Alexa Fluor 568 (white circle). ***B***, Representative data showing the effect of the local application of ATP (left) and glutamate (right). The shaded area indicates the puffed area. ATP induced a glissando, whereas glutamate activated only astrocytes located in the puffed area, and these activities did not propagate. ***C***, Ratios of trials that successfully induced glissando via a local application of ATP and glutamate and electric stimulation (100 pulses at 100 Hz, 100 μs rectangular pulses at 100 μA). The data for four mice are summarized. ***D***, No significant difference in the glissando velocity between spontaneously occurring and ATP-evoked glissandi (Student's t test; $n = 38$ and 8 glissandi, respectively). Error bars indicate SD.

higher magnification, we found that calcium activities propagated from the foot ("leader") of one astrocyte to the neighboring foot ("follower") of another astrocyte (Fig. 4*D*; supplemental Movie 2, available at www.jneurosci.org as supplemental material). Therefore, glissandi are combinatorial of intercellular waves among astrocytes and intracellular waves within astrocytes.

We conducted pharmacological experiments to examine the mechanisms underlying glissandi. Glissandi were completely abolished by tetrodotoxin, a voltage-sensitive sodium channel inhibitor (Fig. 5*A*,*B*). In contrast, tetrodotoxin did not affect the level of sporadic background activities (control: 0.12 ± 0.10 activities/min; tetrodotoxin: 0.11 ± 0.10 activities/min; $t_{(32)} = 0.86$, $p = 0.40$, Student's t test), in agreement with previous reports showing that sporadic activities are intrinsic to astrocytes and independent of neuronal activity (Parri et al., 2001; Aguado et al., 2002; Nett et al., 2002; Takata and Hirase, 2008).

We tested the effects of inhibitors of cellular signals that are known to mediate glia-to-glia communication (Agulhon et al., 2008; Fiacco et al., 2009): carbenoxolone, a gap junction inhibitor, suramin, a purinergic receptor antagonist, MCPG, a metabotropic glutamate receptor antagonist, and DPCPX, an adenosine A_1 receptor antagonist. Carbenoxolone and suramin reduced the frequency of glissandi, but MCPG and DPCPX did not (Fig. 5*B*). Thus, glissandi require gap junctions and ATP receptor activation. To determine whether ATP receptor activation is sufficient to induce glissandi, we injected ATP into the hippocampus (Fig. 6*A*). The effective radius of this local application was up to 150 μm, as confirmed by diffusion of coapplied Alexa Fluor dye. A local application of ATP to the CA1 stratum pyramidale readily induced glissandi (Fig. 6*B*,*C*). ATP-evoked glissandi did not differ in speed compared with glissandi that occurred spontaneously (Fig. 6*D*). A local application of glutamate activated a small number of astrocytes in the puffed area, and these activities did not propagate beyond the application area (Fig. 6*B*,*C*). Electric stimulation, even at high current intensities (100 pulses, 100 Hz, and 100 μA), did not trigger glissandi, although it did activate a few astrocytes around the tip of the electrode (Fig. 6*C*).

Reduced infraslow fluctuation and blood flow during glissandi

Recent studies have suggested that the fMRI-BOLD signal is associated with changes in infraslow potentials (Hinterberger et al., 2003; Nagai et al., 2004; He et al., 2008; Khader et al., 2008; He and Raichle, 2009). Infraslow potentials are the slow end (<0.5 Hz) of the field potential and reflect synchronous synaptic inputs that result in increased multiunit activity and higher-frequency field oscillations (Rebert, 1973; Elbert, 1990; Vanhatalo et al., 2004; He and Raichle, 2009). They are well documented in the neocortex but have also been reported in other brain regions, including the hippocampus (Borodkin Yu et al., 1984; Fell et al., 2007). While imaging glissandi, we recorded LFPs from CA1 stratum pyramidale (Fig. 7*A*). A fast Fourier transform of the LFPs revealed that the power of the infraslow field fluctuations was reduced by 42 ± 8% during glissandi (Fig. 7*B*,*C*). Glissandi were also associated with a decrease in higher-frequency oscillations (Fig. 7*B*,*C*).

To monitor the flow of RBCs in hippocampal capillaries, blood serum was labeled via an intravenous injection of FITC-dextran, a fluorescent angiographic dye. RBCs appeared as nonlabeled dark interpositions between the labeled plasma. In a line-scan image along a vessel (Kuga et al., 2009), a pattern of

oblique black and white stripes was generated in a space-versus-time *XT*-scan plot (Fig. 7*D*), and the velocity of each RBC was determined by dividing the distance it traveled (ΔX) by the time required for travel (ΔT). Capillaries were randomly selected from the field of view to examine glissando-induced modulation of the RBC velocity. In nearly all the vessels tested, the RBC velocity decreased during glissandi, and the mean change was $-12 \pm 9\%$ (Fig. 7*E*) ($n = 32$ vessels). Thus, glissandi are associated with a widespread decrease in blood flow in the brain subregion.

It should be noted that our data could not resolve whether glissandi preceded or followed changes in infraslow potentials and blood flow, because the initiation loci of glissandi could not be identified in the present study; it is probable that the glissandi observed herein were initiated outside and then entered the microscopic field. Thus, we were unable to determine the exact start times of the glissandi. However, our preliminary experiments demonstrate that glissandi are not triggered or facilitated by acute cerebral ischemia induced by acute occlusion of the bilateral common carotid arteries or by intravenous injections of polystyrene latex beads (φ, 20–50 μm) ($n > 25$ mice) (our unpublished data), and we thus speculate that lowering the blood flow is unlikely to induce glissandi.

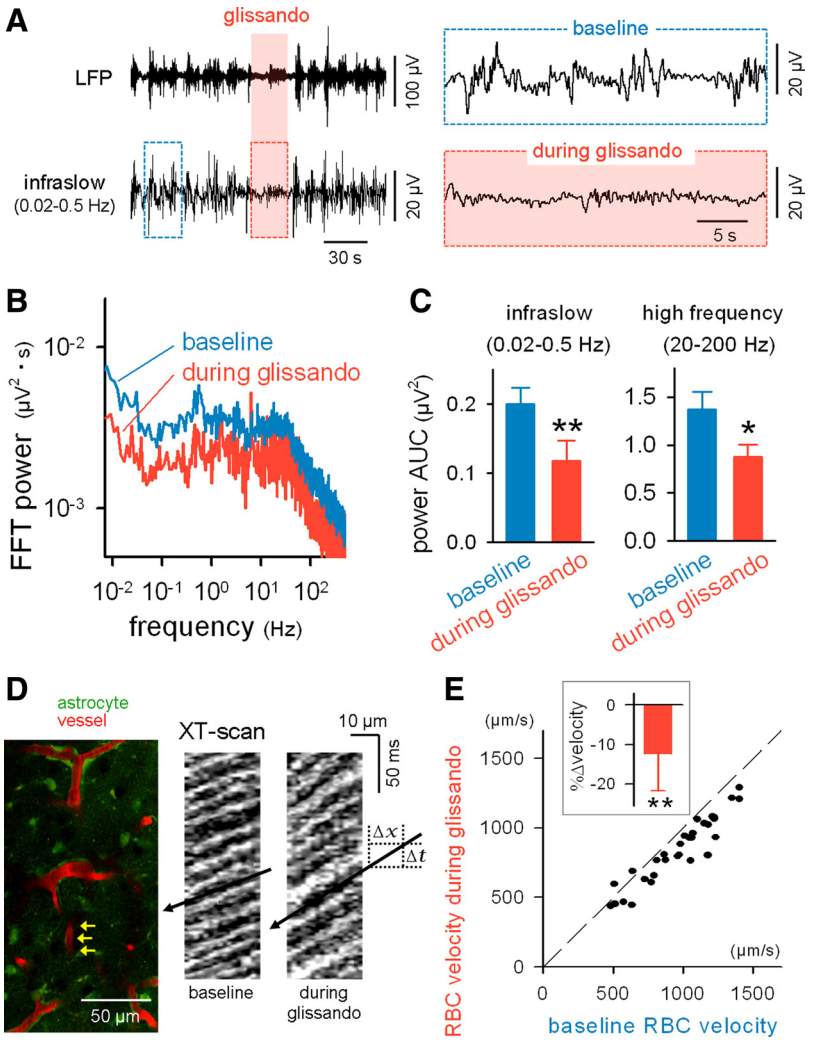

Figure 7. Glissandi are correlated with a reduced infraslow potential and a slowed cerebral vessel flow. ***A***, LFPs were recorded from the CA1 stratum radiatum while monitoring the glissandi. The raw LFP trace (top) was band-filtered (0.02–0.5 Hz) to extract infraslow fluctuations (bottom). Glissandi were generated during the shaded period. The boxed regions are expanded in the insets. ***B***, Fast Fourier transform (FFT) of LFPs during periods of baseline and glissandi. ***C***, During glissandi, the area under the curves (AUCs) of the FFT power decreased in the ranges of 0.02–0.5 and 20–200 Hz. $^*p < 0.05$, $^{**}p < 0.01$ versus baseline ($n = 5$). Error bars indicate SD. ***D***, FITC-dextran was intravenously injected, and astrocytic calcium and blood vessel flows were monitored simultaneously (left). The flow of individual RBCs was measured from capillaries (such as indicated by arrows). Two right kymographs show *XT*-line-scanned images along the longitudinal axes of a capillary during periods of baseline and glissandi. The RBC flow is observed as oblique shadow bands, and the RBC velocity is calculated as the slope $\Delta X/\Delta T$. ***E***, Comparison of the RBC velocity between periods of baseline and glissandi. The dots indicate the data obtained for single capillaries (i.e., single glissandi), and the broken line indicates the diagonal. The inset shows the glissando-induced mean change in RBC velocity. $^{**}p < 0.001$ versus baseline, $t_{(31)} = 7.7$, paired *t* test ($n = 32$ events, 5 mice). Error bars indicate SD.

Discussion

By imaging spontaneous calcium activities from large numbers of astrocytes in the hippocampus *in vivo*, we discovered a large-scale intercellular propagation of calcium waves. These novel collective events coincided with reduced neuronal activity and slower blood vessel flow.

Glissandi as novel dynamics

Several forms of astrocytic calcium waves have been described under artificial or pathological conditions, such as in cultured astrocytes (Cornell-Bell et al., 1990; Charles et al., 1991; Finkbeiner, 1992) and in spreading depression (SD) (Basarsky et al., 1998; Kunkler and Kraig, 1998; Peters et al., 2003; Chuquet et al., 2007). Glissandi differ in several respects from these previously known waves. First, the propagation speed of glissandi was ~60 μm/s, which is faster than any known calcium waves; the wave speeds detected in astrocyte cultures and acute brain slices are 10–20 μm/s (Scemes and Giaume, 2006), and the speeds of SD-related waves are 30–40 μm/s (Peters et al., 2003; Chuquet et al., 2007). Second, glissandi did not occur in the presence of tetrodotoxin; to our knowledge, all the other wave types observed to date are insensitive to tetrodotoxin. For example, cultured astrocytes are capable of generating waves even in the absence of neurons (Cornell-Bell et al., 1990; Charles et al., 1991; Finkbeiner, 1992). Likewise, SD-related waves of astrocytes are not blocked by tetrodotoxin (Chuquet et al., 2007), because SD is an action potential-independent propagation of morbid hyperexcitation that occurs in response to excessive extracellular potassium concentrations. Third, SD is known to cause a marked drop (or complete arrest) in blood flow (Tomita et al., 2005; Chuquet et al., 2007). During glissandi, however, the blood flow decreased by only 10%, which is more likely to be in the physiological range (Kuga et al., 2009). Fourth, the wave-like dynamics previously reported in astrocytes *in vivo* are relatively local events that are restricted to several or tens of adjacent astrocytes and do not regeneratively propagate over long distances (Dombeck et al., 2007; Hoogland et al., 2009; Kuchibhotla et al., 2009; Nimmerjahn et al., 2009).

Glissandi as physiological dynamics

Glissandi are unlikely to result from experimental tissue damage caused by cortex aspiration for the four following reasons. First,

we did not find evidence that our aspiration procedure caused any aberrant or pathological degeneration of the cells—even those located immediately below the aspirated domain. Second, we carefully minimized the volume of the aspirated tissue to avoid reaching the alveus surface of the hippocampus. Thus, the hippocampus was not directly injured by the aspiration. Indeed, glissandi never occurred in intentionally injured preparations in which we aspirated the splenium immediately above the hippocampal alveus ($n = 7$ mice). Third, it is already known that reactive astrocytes in damaged tissues do not exhibit spontaneous calcium activities (Aguado et al., 2002). Finally, glissandi were observed only at laser intensities <10 mW. It is intriguing that no glissandi emerged even at laser intensities of 10–20 mW. This range of laser intensities is sufficiently low to cause no increase in sporadic activities, and thus, it has been used in many previous studies. Our findings indicate that the collective dynamics of astrocytes are far more vulnerable to light than previously thought.

The temperature in the hippocampus was relatively low in our preparations. It is possible that hypothermia enhances the observation probability of glissandi. We attempted to heat the hippocampus by perfusion with warmed aCSF, but we failed to observe glissandi in the perfused hippocampus, regardless of the fluid temperature. Probably, solution perfusion by itself damaged the exposed hippocampus, even though the perfusion speed was reduced to as slow as 0.5 ml/min (range, 0.5–3 ml/min). Thus, we cannot completely rule out the possibility that glissandi reflected pathological responses to hypothermia.

Although the present work focused on the hippocampus, we also detected glissandi in the neocortex. Thus, glissandi may prevail in the cortex. The frequency of the observed glissandi, however, was substantially lower in the neocortex than in the hippocampus; thus far, we have encountered neocortical glissandi only in three mice. We speculate that craniotomy, even if performed with extreme care, may injure the surface of the neocortex, disrupting the delicate dynamics of astrocytes. Thus, the hippocampus was experimentally more suitable to examine the properties of glissandi, rather than the neocortex.

Roles of glissandi

The ability of tetrodotoxin to block glissandi demonstrated that they required neuronal activity. Nonetheless, they were not evoked by electric field stimulation. This ostensible contradiction may be explained by two different interpretations. First, glissandi are triggered by afferents arising from the outside of the hippocampus, such as the entorhinal cortex, septum, and locus ceruleus. The locus ceruleus, in particular, is a fascinating candidate, because this brain region gives rise to noradrenergic axons to the hippocampus and cortex, some of which projections are likely to make direct contacts with astrocytes (Duffy and MacVicar, 1995; Bekar et al., 2008). The effects of ATP may be to induce release from these terminals in addition to direct activation of astrocytes.

Second, glissandi are not merely a reflection of increased or decreased neuronal activity, but rather that they emerge in response to changes in coordinated neuronal network activity. Although electric stimulation readily induces synchronized neuronal activity, it results in indiscriminate activation of neuronal somata, axons, and dendrites surrounding the stimulating electrode tip (Histed et al., 2009). Such artificial activation probably disrupts the intrinsic nature of ongoing network activity. Importantly, one of the prominent features of ongoing neuronal activity is spontaneous state changes (i.e., spontaneous fluctuations in the spatiotemporal patterns of network activity and oscillations) (Fox and Raichle, 2007). Thus, the apparent contradiction can be accounted for by assuming that the state changes trigger glissandi (i.e., by assuming that tetrodotoxin prevents glissandi because it inhibits the intrinsic network oscillations per se). This idea is consistent with two following observations. First, the generation of glissandi is associated with a decrease in the power of infraslow field oscillations (i.e., state changes). Second, we previously found that the effect of electrical stimulation is local and transient and thus cannot induce a persistent shift in the global network state (Sasaki et al., 2007). Given that infraslow potential fluctuations are known to correlate with changes in BOLD signals (Hinterberger et al., 2003; Nagai et al., 2004; He et al., 2008; Khader et al., 2008; He and Raichle, 2009), we speculate that glissandi mediate the activity-dependent, large-scale modulation of cerebral blood flow.

References

Aguado F, Espinosa-Parrilla JF, Carmona MA, Soriano E (2002) Neuronal activity regulates correlated network properties of spontaneous calcium transients in astrocytes in situ. J Neurosci 22:9430–9444.

Agulhon C, Petravicz J, McMullen AB, Sweger EJ, Minton SK, Taves SR, Casper KB, Fiacco TA, McCarthy KD (2008) What is the role of astrocyte calcium in neurophysiology? Neuron 59:932–946.

Agulhon C, Fiacco TA, McCarthy KD (2010) Hippocampal short- and long-term plasticity are not modulated by astrocyte Ca^{2+} signaling. Science 327:1250–1254.

Basarsky TA, Duffy SN, Andrew RD, MacVicar BA (1998) Imaging spreading depression and associated intracellular calcium waves in brain slices. J Neurosci 18:7189–7199.

Bekar LK, He W, Nedergaard M (2008) Locus coeruleus alpha-adrenergic-mediated activation of cortical astrocytes in vivo. Cereb Cortex 18:2789–2795.

Borodkin YuS, Lapina IA, Gogolitsyn YuL (1984) Changes in minute waves of superslow brain activity after various methods for electrostimulating two neocortical zones. Neurosci Behav Physiol 14:373–379.

Charles AC, Merrill JE, Dirksen ER, Sanderson MJ (1991) Intercellular signaling in glial cells: calcium waves and oscillations in response to mechanical stimulation and glutamate. Neuron 6:983–992.

Chuquet J, Hollender L, Nimchinsky EA (2007) High-resolution *in vivo* imaging of the neurovascular unit during spreading depression. J Neurosci 27:4036–4044.

Cornell-Bell AH, Finkbeiner SM, Cooper MS, Smith SJ (1990) Glutamate induces calcium waves in cultured astrocytes: long-range glial signaling. Science 247:470–473.

De Paola V, Arber S, Caroni P (2003) AMPA receptors regulate dynamic equilibrium of presynaptic terminals in mature hippocampal networks. Nat Neurosci 6:491–500.

Dombeck DA, Khabbaz AN, Collman F, Adelman TL, Tank DW (2007) Imaging large-scale neural activity with cellular resolution in awake, mobile mice. Neuron 56:43–57.

Dombeck DA, Harvey CD, Tian L, Looger LL, Tank DW (2010) Functional imaging of hippocampal place cells at cellular resolution during virtual navigation. Nat Neurosci 13:1433–1440.

Duffy S, MacVicar BA (1995) Adrenergic calcium signaling in astrocyte networks within the hippocampal slice. J Neurosci 15:5535–5550.

Elbert T (1990) Slow cortical potentials reflect the regulation of cortical excitability. In: Slow potential changes in the human brain (McCallum WC, Curry SH, eds). New York: Springer.

Fell J, Fritz NE, Burr W, Ludowig E, Axmacher N, Elger CE, Helmstaedter C (2007) Human neocortical and hippocampal near-DC shifts are interconnected. Hippocampus 17:413–419.

Fiacco TA, Agulhon C, Taves SR, Petravicz J, Casper KB, Dong X, Chen J, McCarthy KD (2007) Selective stimulation of astrocyte calcium in situ does not affect neuronal excitatory synaptic activity. Neuron 54:611–626.

Fiacco TA, Agulhon C, McCarthy KD (2009) Sorting out astrocyte physiology from pharmacology. Annu Rev Pharmacol Toxicol 49:151–174.

Finkbeiner S (1992) Calcium waves in astrocytes—filling in the gaps. Neuron 8:1101–1108.

Fox MD, Raichle ME (2007) Spontaneous fluctuations in brain activity ob-

served with functional magnetic resonance imaging. Nat Rev Neurosci 8:700–711.
Giaume C, Koulakoff A, Roux L, Holcman D, Rouach N (2010) Astroglial networks: a step further in neuroglial and gliovascular interactions. Nat Rev Neurosci 11:87–99.
Girouard H, Bonev AD, Hannah RM, Meredith A, Aldrich RW, Nelson MT (2010) Astrocytic endfoot Ca^{2+} and BK channels determine both arteriolar dilation and constriction. Proc Natl Acad Sci U S A 107:3811–3816.
Gordon GR, Choi HB, Rungta RL, Ellis-Davies GC, MacVicar BA (2008) Brain metabolism dictates the polarity of astrocyte control over arterioles. Nature 456:745–749.
Hamilton NB, Attwell D (2010) Do astrocytes really exocytose neurotransmitters? Nat Rev Neurosci 11:227–238.
He BJ, Raichle ME (2009) The fMRI signal, slow cortical potential and consciousness. Trends Cogn Sci 13:302–309.
He BJ, Snyder AZ, Zempel JM, Smyth MD, Raichle ME (2008) Electrophysiological correlates of the brain's intrinsic large-scale functional architecture. Proc Natl Acad Sci U S A 105:16039–16044.
Hinterberger T, Veit R, Strehl U, Trevorrow T, Erb M, Kotchoubey B, Flor H, Birbaumer N (2003) Brain areas activated in fMRI during self-regulation of slow cortical potentials (SCPs). Exp Brain Res 152:113–122.
Hirase H, Qian L, Barthó P, Buzsáki G (2004) Calcium dynamics of cortical astrocytic networks in vivo. PLoS Biol 2:E96.
Histed MH, Bonin V, Reid RC (2009) Direct activation of sparse, distributed populations of cortical neurons by electrical microstimulation. Neuron 63:508–522.
Hoogland TM, Kuhn B, Göbel W, Huang W, Nakai J, Helmchen F, Flint J, Wang SS (2009) Radially expanding transglial calcium waves in the intact cerebellum. Proc Natl Acad Sci U S A 106:3496–3501.
Iadecola C, Nedergaard M (2007) Glial regulation of the cerebral microvasculature. Nat Neurosci 10:1369–1376.
Ikegaya Y, Kim JA, Baba M, Iwatsubo T, Nishiyama N, Matsuki N (2001) Rapid and reversible changes in dendrite morphology and synaptic efficacy following NMDA receptor activation: implication for a cellular defense against excitotoxicity. J Cell Sci 114:4083–4093.
Khader P, Schicke T, Röder B, Rösler F (2008) On the relationship between slow cortical potentials and BOLD signal changes in humans. Int J Psychophysiol 67:252–261.
Kuchibhotla KV, Lattarulo CR, Hyman BT, Bacskai BJ (2009) Synchronous hyperactivity and intercellular calcium waves in astrocytes in Alzheimer mice. Science 323:1211–1215.
Kuga N, Hirata T, Sakai I, Tanikawa Y, Chiou HY, Kitanishi T, Matsuki N, Ikegaya Y (2009) Rapid and local autoregulation of cerebrovascular blood flow: a deep-brain imaging study in the mouse. J Physiol 587:745–752.
Kunkler PE, Kraig RP (1998) Calcium waves precede electrophysiological changes of spreading depression in hippocampal organ cultures. J Neurosci 18:3416–3425.
Mizrahi A, Crowley JC, Shtoyerman E, Katz LC (2004) High-resolution *in vivo* imaging of hippocampal dendrites and spines. J Neurosci 24:3147–3151.
Nagai Y, Critchley HD, Featherstone E, Fenwick PB, Trimble MR, Dolan RJ (2004) Brain activity relating to the contingent negative variation: an fMRI investigation. Neuroimage 21:1232–1241.
Nett WJ, Oloff SH, McCarthy KD (2002) Hippocampal astrocytes in situ exhibit calcium oscillations that occur independent of neuronal activity. J Neurophysiol 87:528–537.
Nimmerjahn A, Kirchhoff F, Kerr JN, Helmchen F (2004) Sulforhodamine 101 as a specific marker of astroglia in the neocortex in vivo. Nat Methods 1:31–37.
Nimmerjahn A, Mukamel EA, Schnitzer MJ (2009) Motor behavior activates Bergmann glial networks. Neuron 62:400–412.
Ohiorhenuan IE, Mechler F, Purpura KP, Schmid AM, Hu Q, Victor JD (2010) Sparse coding and high-order correlations in fine-scale cortical networks. Nature 466:617–621.
Olshausen BA, Field DJ (2004) Sparse coding of sensory inputs. Curr Opin Neurobiol 14:481–487.
Parpura V, Basarsky TA, Liu F, Jeftinija K, Jeftinija S, Haydon PG (1994) Glutamate-mediated astrocyte-neuron signalling. Nature 369:744–747.
Parri HR, Gould TM, Crunelli V (2001) Spontaneous astrocytic Ca^{2+} oscillations in situ drive NMDAR-mediated neuronal excitation. Nat Neurosci 4:803–812.
Peters O, Schipke CG, Hashimoto Y, Kettenmann H (2003) Different mechanisms promote astrocyte Ca^{2+} waves and spreading depression in the mouse neocortex. J Neurosci 23:9888–9896.
Rebert CS (1973) Slow potential correlates of neuronal population responses in the cat's lateral geniculate nucleus. Electroencephalogr Clin Neurophysiol 35:511–515.
Sasaki T, Matsuki N, Ikegaya Y (2007) Metastability of active CA3 networks. J Neurosci 27:517–528.
Sasaki T, Kuga N, Namiki S, Matsuki N, Ikegaya Y (2011) Locally synchronized astrocytes. Cereb Cortex. Advance online publication. Retrieved January 18, 2011. doi:10.1093/cercor/bhq256.
Scemes E, Giaume C (2006) Astrocyte calcium waves: what they are and what they do. Glia 54:716–725.
Takata N, Hirase H (2008) Cortical layer 1 and layer 2/3 astrocytes exhibit distinct calcium dynamics in vivo. PLoS One 3:e2525.
Tomita M, Schiszler I, Tomita Y, Tanahashi N, Takeda H, Osada T, Suzuki N (2005) Initial oligemia with capillary flow stop followed by hyperemia during K^+-induced cortical spreading depression in rats. J Cereb Blood Flow Metab 25:742–747.
Vanhatalo S, Palva JM, Holmes MD, Miller JW, Voipio J, Kaila K (2004) Infraslow oscillations modulate excitability and interictal epileptic activity in the human cortex during sleep. Proc Natl Acad Sci U S A 101:5053–5057.
Wang X, Lou N, Xu Q, Tian GF, Peng WG, Han X, Kang J, Takano T, Nedergaard M (2006) Astrocytic Ca^{2+} signaling evoked by sensory stimulation in vivo. Nat Neurosci 9:816–823.
Wolfe J, Houweling AR, Brecht M (2010) Sparse and powerful cortical spikes. Curr Opin Neurobiol 20:306–312.

Large-scale calcium waves traveling through astrocytic networks *in vivo*

Nahoko Kuga, Takuya Sasaki, Yuji Takahara, Norio Matsuki, and Yuji Ikegaya

This file includes:

3 Supplemental Figures

Legends of 2 Movies

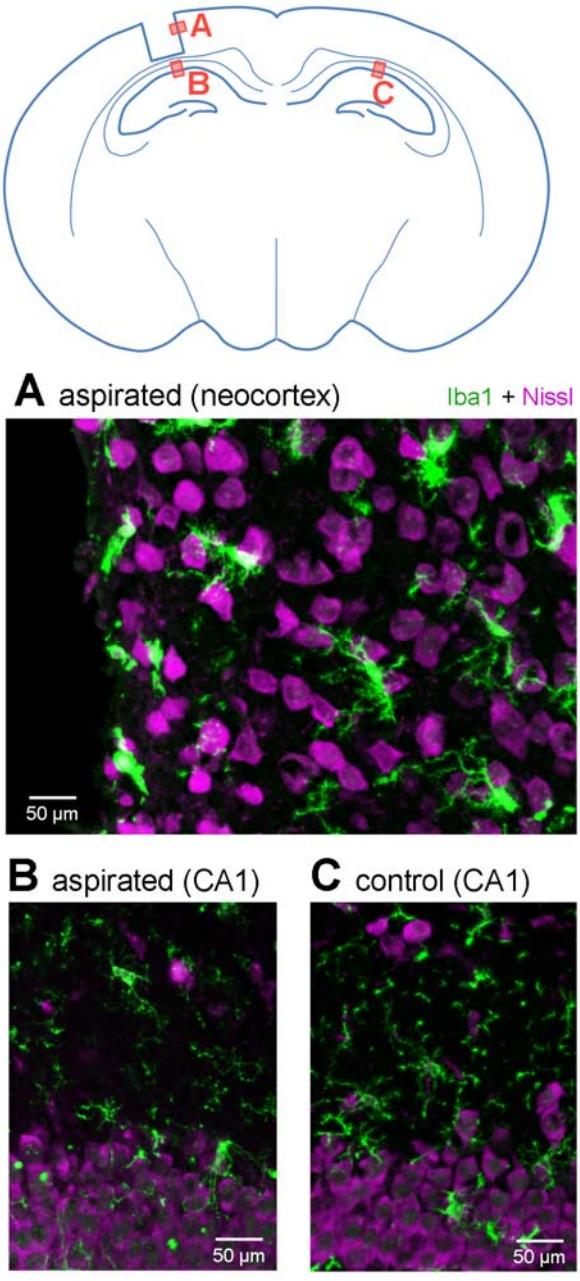

Fig. S1. Neocortical aspiration does not activate hippocampal microglia by neocortical aspiration. Comparison of Iba1-positive cells in the hippocampal CA1 stratum oriens between aspirated (*B*) and the contralateral (*C*) side. Fluorescent Nissl (magenta) was used for counterstaining. No upregulation of Iba1 occurred after aspiration, whereas the wall of the exposed neocortex (positive control) exhibited an increased level of Iba1 expression (*A*).

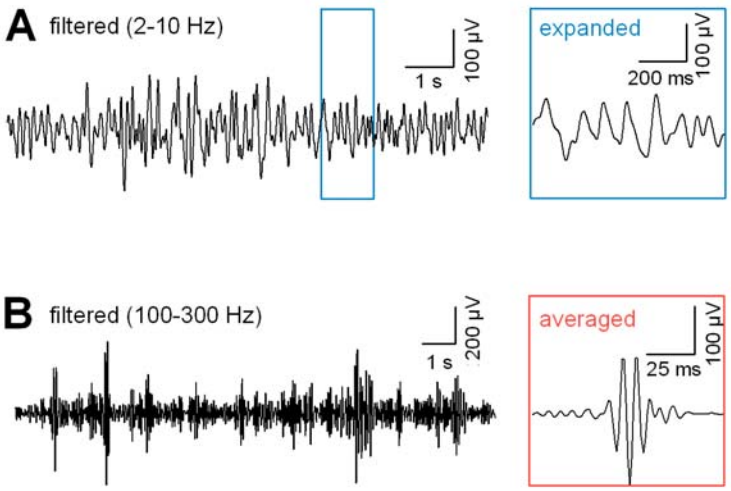

Fig. S2. Exposed hippocampi exhibit the normal patterns of local field potentials. *A*, Representative traces of theta oscillations recorded from the CA1 pyramidal cell layer in the hippocampus that received aspiration of the ipsilateral neocortex. The raw trace was band-pass filtered in the 2−10 Hz range, so that theta waves were identifiable. The boxed region was time-magnified in the *right* inset. *B*, Representative ripple waves. Traces were band-pass filtered in the 100−300 Hz range. The trace in the *right* box shows the ripple-triggered average of local field potentials. Theta and ripple waves were commonly observed in all 5 animals tested.

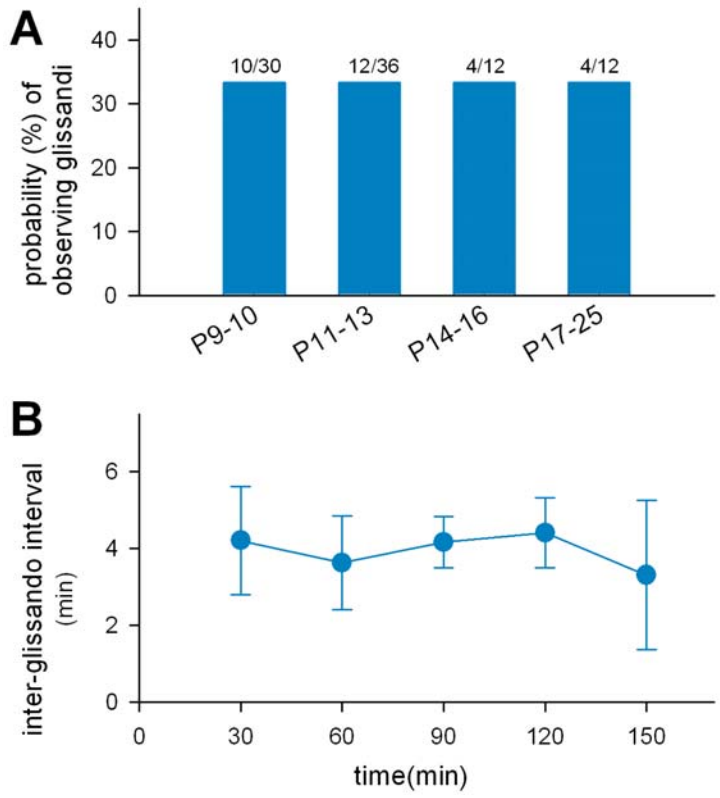

Fig. S3. Occurrence of glissandi does not depend on animals' ages or the time period of optical imaging. *A*, The probability of observing glissandi did not differ depending on the ages of animals ranging from postnatal day 9 to 25. The fraction above each data bar represents the number of animals that showed glissandi over the number of animals tested. All data were obtained at laser intensities of less than 10 mV. *B*, The frequency of glissando occurrence did not change during our observation period of 30−150 min after the start of imaging. The glissando frequency was measured by the mean time interval from the onset of one glissando to that of the next glissando (n = 6 mice). .

Movie S1 Glissando in hippocampal astrocytes. A Kalman-filtered raw fluorescence image is followed by a $\Delta F/F$ movie that includes a glissando. The movie speed is 100-fold faster than real time. The movie size corresponds to a rectangle of 416 μm × 354 μm.

Movie S2 Original movie of Fig. 4D showing foot-to-foot activity propagation during a glissando. The movie speed is in real time.